

TIME-DEPENDENT TRANSPORT IN INTERACTING MESOSCOPIC SYSTEMS

A. P. Jauho

Mikroelektronik Centret

Technical University of Denmark, Ørsteds Plads, Bldg. 345east,

DK-2800 Kgs. Lyngby, Denmark

E-mail: antti@mic.dtu.dk

We review recent applications of the nonequilibrium Green function technique to time-dependent transport in mesoscopic semiconductor systems.

1 Introduction

The study of mesoscopic phenomena is one of the most active areas of today's solid state physics. One can observe signatures of mesoscopics in a large number of different physical systems, and a comprehensive review would not be appropriate in the present context. The present volume focuses on Kadanoff–Baym–Keldysh Green functions, and consequently we restrict ourselves to certain examples which have been studied with the help of these techniques. The generic system we have in mind is a semiconductor heterostructure where charge carriers are introduced either by modulation doping, or they flow in and out of the system through metallic or superconducting contacts. Transport physics in these systems can roughly be divided into two categories: perpendicular transport and parallel transport, according to whether the charge carriers' motion is perpendicular or parallel to the layers that form the heterostructures. A representative example of perpendicular transport is the resonant-tunneling diode (RTD), which consists of alternate layers of semiconductor materials with different band gaps; a schematic conduction band diagram is shown in Fig.1. Charge carriers entering from left may, at a certain bias voltage, be tuned to the quasibound state in the quantum well, which results in a large enhancement of the transmitted current. At off-resonance conditions only a small current can flow, because transmission through the classically inaccessible regions is exponentially suppressed. This leads to a nonmonotonic current-voltage characteristic, and a number of device applications have been proposed, whose operating principles are based on this property.

In the case of parallel transport much attention has been devoted to quantum point contacts (QPC), see Fig.2 for a typical experimental configuration, and other structures based on similar ideas. Here the key ingredient is metallic gates that are deposited on the heterostructure; by adjusting the gate po-

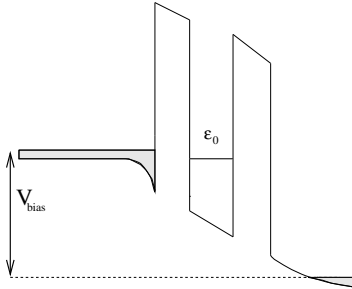


Figure 1: Double-barrier semiconductor heterostructure biased close to resonance, where charge carriers emerging from the source contact are matched to the energy of the quasibound state ϵ_0 in the quantum well. Occupied contact states are shown as hatched, and the band bending is due to charge accumulation or depletion.

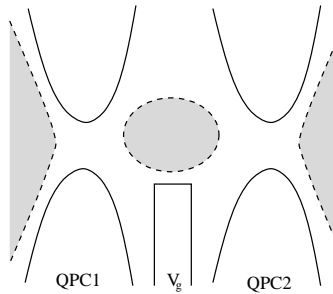


Figure 2: Coulomb island, which consists of two tunable quantum point contacts QPC1 and QPC2, and a side gate which allows one to vary the chemical potential, and hence the charge density in the central region. The two-dimensional electron gas underlying the gate structure is depleted outside the hatched regions.

tentials it is possible to deplete the underlying two-dimensional electron gas, and thus introduce spatial modulations of the two-dimensional charge density. Quantum point contacts are based on a split gate geometry: here, at sufficiently high negative gate voltages, the effective connection between the two unmodulated electron gases (“source” and “drain”) is so narrow that perpendicular mode quantization becomes observable, and the measured conductance is an integer multiple of the quantum unit of conductance, e^2/h . In later sections we describe simple models pertaining to structures like the one shown in Fig.2.

The hallmark of mesoscopic phenomena is the phase coherence of the charge carriers, which is maintained over a significant part of the transport

process. The interference effects resulting from this phase coherence are reflected in a number of experimentally measurable properties. Weak localization can be understood as an increased return probability (and hence increased resistance) due to *coherent* backscattering of charge carriers. Another example where phase coherence is central is the Aharonov–Bohm effect, where interference of two different transport paths in a ring geometry results in an oscillatory magnetoresistance. Yet another example is universal conductance fluctuations, where the conductance of a sample displays rapid changes on the scale of e^2/h (hence the “universality”) when an external control parameter is changed. The external parameter could be magnetic field, or thermal cycling, and the fluctuations reflect changes in the conducting channels either due to different impurity configurations (thermal cycling), or differences in the way the conduction channels are located in the sample (magnetic field). In these notes we focus on an alternative way of affecting the phase coherence: external *time-dependent* perturbations. The interplay of external time dependence and phase coherence can be phenomenologically understood as follows. If the single-particle energies acquire a time dependence, then the wavefunctions have an extra phase factor, $\psi \sim \exp[-i \int^t dt' \varepsilon(t')]$. For a uniform system such an overall phase factor is of no consequence. However, if the external time dependence is different in different parts of the system, and the particles can move between these regions (without being “dephased” by inelastic collisions), the phase difference becomes important.

The interest in time-dependent mesoscopic phenomena stems from recent progress in several experimental techniques. Time dependence is a central ingredient in many different experiments, of which we mention the following: (i) *Single-electron pumps and turnstiles*. Here, time-modified gate signals move electrons one by one through a quantum dot, leading to a current which is proportional to the frequency of the external signal. These structures have considerable importance as current standards. The Coulombic repulsion of the carriers in the central region is crucial to the operational principle of these devices, and underlines the fact that extra care must be paid to interactions when considering time-dependent transport in mesoscopic systems. (ii) *ac response and transients in resonant-tunneling devices*. Resonant tunneling devices (RTD) have a number of applications as high-frequency amplifiers or detectors. For the device engineer, a natural approach would be to model these circuit elements with resistors, capacitances, and inductors. The question then arises as to what, if any, are the appropriate “quantum” capacitances and inductances one should ascribe to these devices. Answering this question requires the use of time-dependent quantum-transport theory.

A central issue will be the treatment of interactions in the mesoscopic

region, and, as we shall see, nonequilibrium Green function techniques are well suited for this purpose. First analyses of tunneling problems in nonequilibrium systems were performed already in the 70s by Caroli and co-workers^{1,2,3,4}. In later years the steady state situation has been addressed by a large number of papers, however the literature on time-dependent nonequilibrium transport treated with Green functions is much more restricted than in the stationary case (see the recent text-book by Haug and Jauho⁵ for extensive references for works published before 1996; this review will concentrate on some of the more recent advances. Additional useful and related information can also be found in the monograph by Datta⁶).

Among the central results obtained with the nonequilibrium Green function techniques is that under certain conditions (to be discussed below) a Landauer-type conductance formula^{7,8} can be derived. The Landauer formula relates the conductance g of a mesoscopic sample [which is connected via “ideal” leads to two (or more) reservoirs] to its transmission properties, $g = (e^2/h)T$, where T is the quantum mechanical transmission coefficient of the sample. Conductance formulae have played an important role in the analysis of many mesoscopic transport phenomena, and it is therefore of interest to investigate whether interactions and/or time-dependence can be treated in a similar fashion. This study forms the core of the present review.

2 Nonequilibrium formulation of tunneling physics

The total current measured in an external ammeter can be split into two contributions: the current flowing into the mesoscopic region, and the current flowing in and out of the accumulation or depletion regions in the leads, i.e., the displacement or capacitive current. We begin by deriving an expression for the tunneling current, and comment on models for the displacement current later. One should also note that the displacement current does not contribute to the time averaged current, which is often the experimentally relevant quantity. We shall also assume that the electric fields in the leads are effectively screened out, so that the voltage drop occurs across the mesoscopic region. This assumption sets an upper bound for the external driving frequency, which should not exceed the plasma frequency. Estimates for the cut-off frequency are in the range of 10 GHz – 1 THz, depending on the device geometry and dimensionality⁹, which are sufficiently high for most present applications.

We recall that the basic difference between construction of equilibrium and nonequilibrium perturbation schemes is that in nonequilibrium one cannot assume that the system returns to its ground state (or a thermodynamic equilibrium state at finite temperatures) as $t \rightarrow +\infty$. Irreversible effects break

the symmetry between $t = -\infty$ and $t = +\infty$, and this symmetry is heavily exploited in the derivation of the equilibrium perturbation expansion^{10,11,12}. In nonequilibrium situations one can circumvent this problem by allowing the system to evolve from $-\infty$ to the moment of interest (for definiteness, let us call this instant t_0), and then continues the time evolution from $t = t_0$ back to $t = -\infty$. The advantage of this procedure is that all expectation values are defined with respect to a well-defined state, i.e., the state in which the system was prepared in the remote past. The price is that one must treat the two time branches on an equal footing.

In the context of tunneling problems the nonequilibrium formalism works as follows. In the remote past the contacts (i.e., the left and right lead) and the central region are decoupled, and each region is in thermal equilibrium. The equilibrium distribution functions for the three regions are characterized by their respective chemical potentials; these do not have to coincide nor are the differences between the chemical potentials necessarily small. The couplings between the different regions are then established and treated as perturbations via the standard techniques of perturbation theory, albeit on the two-branch time contour. It is important to notice that the couplings do not have to be small, e.g., with respect level to spacings or $k_B T$, and typically must be treated to all orders.

3 Current formulas

We can now present the mathematical formulation of the problem. A detailed presentation can be found in a recent text-book⁵, and here we present just some of the central ideas. The contacts are assumed to be noninteracting, and the single-particle energy in lead α is given by

$$\varepsilon_{k,\alpha}(t) = \epsilon_{k,\alpha} + \Delta_\alpha(t), \quad (1)$$

where $\Delta_\alpha(t)$ is the external time modulation. The leads are connected to the central (or, mesoscopic) region via a hopping term with matrix element $V_{k\alpha;n}(t)$, where n labels the eigenstates of the central region. Collecting the various terms results in the Hamiltonian $H = H_L + H_R + H_T + H_{\text{cen}}$, or, explicitly:

$$H = \sum_{k,\alpha} \epsilon_{k,\alpha}(t) c_{k,\alpha}^\dagger c_{k,\alpha} + \sum_{k,\alpha;n} \left[V_{k\alpha;n}(t) c_{k,\alpha}^\dagger d_n + \text{h.c.} \right] + H_{\text{cen}} [\{d_n\}, \{d_n^\dagger\}, t], \quad (2)$$

where the central part Hamiltonian must be chosen according to the system under consideration. The operators $\{d_n\}, \{d_n^\dagger\}$ refer to a complete set of single-particle states of the central region. The derivation of the basic formula for

the time-dependent current does not require an explicit form for H_{cen} ; the actual evaluation of the formula of course requires this information. We write $H_{\text{cen}} = \sum_n \epsilon_n(t) d_n^\dagger d_n + H_{\text{int}}$, where H_{int} could be electron-phonon interaction, or an Anderson impurity:

$$H_{\text{int}}^{\text{el-ph}} = \sum_{n\sigma} d_{n,\sigma}^\dagger d_{n,\sigma} \sum_{\mathbf{q}} M_{n,\mathbf{q}} [a_{\mathbf{q}}^\dagger + a_{\mathbf{q}}] \quad (3)$$

$$H_{\text{int}}^A = U \sum_n d_{n,\uparrow}^\dagger d_{n,\uparrow} d_{n,\downarrow}^\dagger d_{n,\downarrow}. \quad (4)$$

According to the basic ideas of the tunneling approach presented above, the occupations of the leads are determined by equilibrium distribution functions. Thus the Green functions for the contacts are known explicitly:

$$\begin{aligned} g_{k\alpha}^<(t, t') &\equiv i \langle \mathbf{c}_{k\alpha}^\dagger(t') \mathbf{c}_{k\alpha}(t) \rangle \\ &= i f(\epsilon_{k\alpha}^0) \exp \left[-i \int_{t'}^t dt_1 \epsilon_{k\alpha}(t_1) \right], \end{aligned} \quad (5)$$

$$\begin{aligned} g_{k\alpha}^{r,a}(t, t') &\equiv \mp i \theta(\pm t \mp t') \langle \{ \mathbf{c}_{k\alpha}(t), \mathbf{c}_{k\alpha}^\dagger(t') \} \rangle \\ &= \mp i \theta(\pm t \mp t') \exp \left[-i \int_{t'}^t dt_1 \epsilon_{k\alpha}(t_1) \right]. \end{aligned} \quad (6)$$

We start the derivation by considering the current leaving the, e.g., left contact, and entering the central region:

$$J_L(t) = \langle I_L(t) \rangle = \langle (-e) \dot{N}_L(t) \rangle = -ie \langle [H, N_L] \rangle. \quad (7)$$

The commutator $[H, N_L]$ is readily evaluated, and one finds

$$J_L(t) = \frac{2e}{\hbar} \text{Re} \left\{ \sum_{k,\alpha,n} V_{k\alpha,n}(t) G_{n,k\alpha}^<(t, t) \right\}, \quad (8)$$

which involves the time-diagonal part of the correlation function

$$G_{n,k\alpha}^<(t, t') = i \langle c_{k\alpha}^\dagger(t') d_n(t) \rangle. \quad (9)$$

The next step consist of writing down the equation-of-motion for the time-ordered function $G_{n,k\alpha}^t(t, t')$, and a subsequent analytic continuation with the Langreth rules¹³ leads to

$$G_{n,k\alpha}^<(t, t') = \sum_m \int dt_1 V_{k\alpha,m}^* \left[G_{nm}^r(t, t_1) g_{k\alpha}^<(t_1, t') + G_{nm}^<(t, t_1) g_{k\alpha}^a(t_1, t') \right]. \quad (10)$$

Substituting the expressions for the contact Green functions, Eqs.(5)–(6) finally yields

$$J_L(t) = -\frac{2e}{\hbar} \int_{-\infty}^t dt_1 \int \frac{d\epsilon}{2\pi} \text{ImTr} \left\{ e^{-i\epsilon(t_1-t)} \mathbf{\Gamma}^L(\epsilon, t_1, t) \right. \\ \left. \times [\mathbf{G}^<(t, t_1) + f_L^0(\epsilon) \mathbf{G}^r(t, t_1)] \right\}. \quad (11)$$

Here the Green functions $\mathbf{G}^{<,r}$ are *matrices* in the indices (m, n) , and the linewidth functions $\mathbf{\Gamma}$ are defined as

$$[\mathbf{\Gamma}^L(\epsilon, t_1, t)]_{mn} = 2\pi \sum_{\alpha \in L} \rho_\alpha(\epsilon) V_{\alpha,n}(\epsilon, t) V_{\alpha,m}^*(\epsilon, t_1) \exp \left[-i \int_t^{t_1} dt_2 \Delta_\alpha(\epsilon, t_2) \right], \quad (12)$$

where $\rho_\alpha(\epsilon)$ is the density of states. Equation (11) is the main formal result of this report: the subsequent sections are devoted to exploring its special applications. It is important to note that the current formula only involves the Green function of the central region. However, $\mathbf{G}^<(t, t_1)$ must be calculated in the presence of the coupling to the leads, which is a highly nontrivial task for an interacting system. Thus, Eq.(11) can be viewed as a rather formal statement, but nevertheless it provides under many circumstances a very convenient starting-point for further calculations.

4 Special cases

4.1 Stationary limit

In the stationary limit Eq.(11) can be further simplified and we get the result first reported in Ref.¹⁴:

$$J = \frac{ie}{2\hbar} \int \frac{d\epsilon}{2\pi} \text{Tr} \left\{ [\mathbf{\Gamma}^L(\epsilon) - \mathbf{\Gamma}^R(\epsilon)] \mathbf{G}^<(\epsilon) \right. \\ \left. + [f_L^0(\epsilon) \mathbf{\Gamma}^L(\epsilon) - f_R^0(\epsilon) \mathbf{\Gamma}^R(\epsilon)] [\mathbf{G}^r(\epsilon) - \mathbf{G}^a(\epsilon)] \right\} \quad (13)$$

$$= \frac{ie}{\hbar} \int \frac{d\varepsilon}{2\pi} [f_L(\varepsilon) - f_R(\varepsilon)] \mathcal{T}(\varepsilon), \quad (14)$$

where

$$\mathcal{T}(\varepsilon) = \text{Tr} \left\{ \frac{\mathbf{\Gamma}^L(\varepsilon) \mathbf{\Gamma}^R(\varepsilon)}{\mathbf{\Gamma}^L(\varepsilon) + \mathbf{\Gamma}^R(\varepsilon)} [\mathbf{G}^r(\varepsilon) - \mathbf{G}^a(\varepsilon)] \right\}. \quad (15)$$

Equation (14) holds for the special case when the couplings between the left and right leads are proportional (a constant coupling, occurring in the wide-band

limit is a frequently encountered special case). The ratio in the curly brackets in Eq.(15) is well-defined because the $\mathbf{\Gamma}$ -matrices are, by assumption, proportional. The difference between the retarded and advanced Green functions is essentially the density of states. Despite the apparent similarity of Eq.(14) to the Landauer formula, it is important to bear in mind that, in general, there is no immediate connection between the quantity $\mathcal{T}(\varepsilon)$ and the transmission coefficient $T(\varepsilon)$. In particular, when inelastic scattering is present, there is no such connection. These expressions for the stationary current have a wide range of applicability for calculations of current-voltage relations in mesoscopic structures. Recent applications include nonlinear current-voltage calculations¹⁵, transport in carbon nanotubes^{16,17}, Kondo physics^{18,19,20,21,22}, Andreev scattering in semiconductor–superconductor hybrid systems²³ (we return to these two topics below), tunneling through magnetic barriers²⁴, delocalization of excitons in disordered systems²⁵, role of correlations in transport through quantum dots or artificial molecules^{26,27,28,29,30,31,32}, physics of nanowires^{33,34}, analysis of STM (Scanning Tunneling Microscope) experiments^{35,36}, and many others.

4.2 Noninteracting electrons

Now $H_{\text{cen}} = \epsilon_0(t)d^\dagger d = [\epsilon_0 + \Delta_0(t)]d^\dagger d$ (we examine only the single-level case; a generalization to many levels and/or spin is straightforward, all the results are formally the same but the Green functions, self-energies etc. must be interpreted as matrices), and we can give the following explicit results for the occupation $N(t) = -iG^<(t, t)$, and the current $J_{L/R}(t)$ ⁹:

$$N(t) = \sum_{L/R} \int \frac{d\epsilon}{2\pi} f_{L/R}^0(\epsilon) |A_{L/R}(\epsilon, t)|^2 \quad (16)$$

$$J_{L/R}(t) = -\frac{e}{\hbar} \Gamma_{L/R} \left[N(t) + \frac{1}{\pi} \int d\epsilon f_{L/R}^0(\epsilon) \text{Im} \{ A_{L/R}(\epsilon, t) \} \right], \quad (17)$$

where

$$\begin{aligned} A_{L/R}(\epsilon, t) &= \int dt_1 e^{i\epsilon(t-t_1)} e^{-i \int_{t_1}^{t_1} dt_2 \Delta_{L/R}(t_2)} G^r(t, t_1) \\ &= e^{-i \frac{\Delta_0}{\gamma} \sin(\gamma t)} \sum_{k=-\infty}^{\infty} \frac{J_k [(\Delta_0 - \Delta_{L/R})/\gamma] e^{ik\gamma t}}{\epsilon - \epsilon_0 - k\gamma + i\Gamma/2}, \end{aligned} \quad (18)$$

where J_k is the k :th order Bessel function, and we assumed a harmonic time-variation: $\Delta_0(t) = \cos(\gamma t)$. Figures 3 and 4 give a numerical example. We

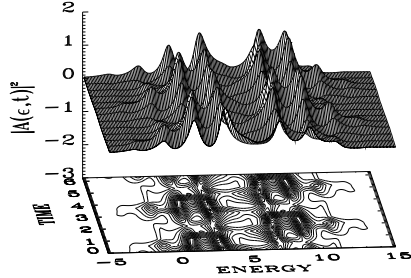


Figure 3: $|A(\epsilon, t)|^2$ as a function of time for harmonic modulation for a symmetric structure, $\Gamma_L = \Gamma_R = \Gamma/2$. The unit for the time-axis is \hbar/Γ , and all energies are measured in units of Γ , with the values $\mu_L = 10$, $\mu_R = 0$, $\epsilon_0 = 5$, $\Delta = 5$, $\Delta_L = 10$, and $\Delta_R = 5$. The modulation frequency is $\omega = 2\Gamma/\hbar$.

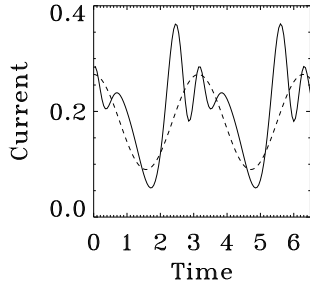


Figure 4: The time-dependent current $J(t)$ for harmonic modulation. The dc bias is defined via $\mu_L = 10$ and $\mu_R = 0$, respectively. The dotted line shows (not drawn to scale) the time dependence of the drive signal. The temperature is $k_B T = 0.1\Gamma$.

draw attention to the maxima in the plot for $|A|^2$; these are related to photonic side-bands occurring at $\epsilon = \epsilon_0 \pm k\omega$ ³⁷. More work along similar lines can be found, e.g., in Ref.³⁸ Bearing in mind the complex structure seen in Fig. 3 it is not surprising that the current in Fig. 4 displays a non-adiabatic time-dependence. The basic physical mechanism underlying the secondary maxima and minima in the current is the line-up of a photon-assisted resonant tunneling peak with the contact chemical potentials.

4.3 Average current

For constant couplings to leads a very simple result can be obtained for the average current:

$$\langle J_L(t) \rangle = \frac{\Gamma_L \Gamma_R}{\Gamma_L + \Gamma_R} \text{Tr} \left\{ -\frac{2e}{\hbar} \int \frac{d\epsilon}{2\pi} \langle \text{Im} \mathbf{A}(\epsilon, t) \rangle [f_L^0(\epsilon) - f_R^0(\epsilon)] \right\}. \quad (19)$$

In the noninteracting single-level case $\langle \text{Im} A(\epsilon, t) \rangle$ is given by

$$\langle \text{Im} A_{L/R}(\epsilon, t) \rangle = -\frac{\Gamma}{2} \sum_{k=-\infty}^{\infty} \frac{J_k^2 [(\Delta_0 - \Delta_{L/R})/\omega]}{(\epsilon - \epsilon_0 - k\omega)^2 + (\Gamma/2)^2}. \quad (20)$$

We shall use these expressions below.

4.4 Resonant tunneling with phonons

Resonant tunneling diodes (see Fig. 1) are important both for technical applications, such as oscillators or infra-red detectors, but they are equally important conceptually as a very clear-cut example of a system exhibiting interacting, far-from equilibrium transport phenomena. In this subsection we consider electron-phonon interactions. As explained in the Introduction, the IV-characteristic is dominated by a maximum when the quasibound state is aligned with the energies of the incoming electrons. Experimentally, however, it was found³⁹ that the current-voltage characteristic could also display a secondary maximum, i.e. a satellite of the main feature. The reason is interaction with phonons: an electron, which approaches the double-barrier structure with a nonresonant energy, can be tuned in the energy of the quasibound state in the quantum well by emitting (or absorbing) an optical phonon, and thus become resonant with an enhanced transmission probability, and increased current. The central-region Hamiltonian (3) is a mathematical formulation for this physical picture.

For simplicity, we consider only energy-independent level-widths Γ_L and Γ_R , when the current (14) becomes

$$J = \frac{e}{\hbar} \frac{\Gamma^L \Gamma^R}{\Gamma^L + \Gamma^R} \int \frac{d\epsilon}{2\pi} [f_L(\epsilon) - f_R(\epsilon)] \int_{-\infty}^{\infty} dt e^{i\epsilon t} A(t), \quad (21)$$

where $A(t) = i[G^r(t) - G^a(t)]$ is the interacting spectral function. In general, an exact evaluation of $A(t)$ is not possible, however, if one neglects the coupling to the contacts (or treats the coupling phenomenologically by introducing an exponential decay in $A(t)$), $G^r(t)$ [and hence $A(t)$] can be calculated exactly⁴⁰.

A very convenient way to calculate $A(t)$ is to use the linked-cluster theorem¹⁰. We write the electron-phonon interaction in the interaction picture (for simplicity we again consider just one level),

$$H_{\text{int}}^{\text{el-ph}}(t) = d^\dagger d \sum_{\mathbf{q}} M_{\mathbf{q}} [a_{\mathbf{q}}^\dagger e^{-i\omega_{\mathbf{q}}t} + a_{\mathbf{q}} e^{i\omega_{\mathbf{q}}t}] . \quad (22)$$

$H_{\text{int}}^{\text{el-ph}}(t)$ can then be viewed as an effective one-electron Hamiltonian in a time-dependent Schrödinger equation, the solution of which gives $A(t)$ (the averaging is now over the phonon subsystem):

$$\begin{aligned} A(t) &= e^{-i\epsilon_0 t} \langle T \{ \exp[-i \int_0^t dt_1 H_{\text{int}}^{\text{el-ph}}(t_1)] \} \rangle \\ &= e^{-i\epsilon_0 t} \exp[-\frac{1}{2} \int_0^t dt_1 \int_0^t dt_2 \langle T \{ H_{\text{int}}^{\text{el-ph}}(t_1) H_{\text{int}}^{\text{el-ph}}(t_2) \} \rangle] , \end{aligned} \quad (23)$$

where T is the time-ordering operator, and we used the linked-cluster theorem on the second line. The time-ordered product is nothing but the free phonon Green function:

$$i \langle T \{ H_{\text{int}}^{\text{el-ph}}(t_1) H_{\text{int}}^{\text{el-ph}}(t_2) \} \rangle = (N+1) e^{-i\omega_{\mathbf{q}}|t_1-t_2|} + N e^{i\omega_{\mathbf{q}}|t_1-t_2|} , \quad (24)$$

where $N = 1/[\exp(\hbar\omega_{\mathbf{q}}\beta) - 1]$. The time-integrals are easily worked out with the result

$$A(t) = \exp[-it(\epsilon_0 - \Delta) - \Phi(t) - \Gamma|t|/2] , \quad (25)$$

where

$$\Delta = \sum_{\mathbf{q}} \frac{M_{\mathbf{q}}^2}{\omega_{\mathbf{q}}} , \quad (26)$$

$$\Phi(t) = \sum_{\mathbf{q}} \frac{M_{\mathbf{q}}^2}{\omega_{\mathbf{q}}^2} [N_{\mathbf{q}}(1 - e^{i\omega_{\mathbf{q}}t}) + (N_{\mathbf{q}} + 1)(1 - e^{-i\omega_{\mathbf{q}}t})] . \quad (27)$$

When substituted in the expression for current, one recovers the result of Wingreen et al.⁴¹, which originally was derived by analyzing the much more complex two-particle Green function

$$G(\tau, s, t) = \theta(s)\theta(t) \langle d(\tau-s)d^\dagger(\tau)d(t)d^\dagger(0) \rangle . \quad (28)$$

The advantage of the method presented here is that one only needs the *single*-particle Green function to use the interacting current formula (14). Other

systematic approaches to the single-particle Green function can therefore be directly applied to the current (e.g., perturbation theory in the tunneling Hamiltonian; Anda and Flores⁴², Hyldgaard et al.⁴³). The model studied in this section is quite flexible and it has been used to describe many other interaction mechanisms in double-barrier systems, such as light assisted magnetotunneling⁴⁴, or plasmon assisted tunneling⁴⁵.

4.5 Multiterminal generalization and displacement current

We now return to the issues of current partition and displacement current in a multiprobe sample, mentioned in the Introduction. The dc situation has been exhaustively analyzed, starting from the seminal work of Büttiker et al⁴⁶. The time-dependent case is more complicated: not only has the tunneling current to be considered, but also the displacement contributions must be accounted for. These issues are essential for two reasons: i) Current conservation and ii) Gauge invariance. (Gauge invariance means that a uniform shift of all voltages should not affect the final results.) A linear, low frequency theory was developed by Büttiker and co-workers⁴⁷, based on an generalization of the scattering matrix formulation of transport theory. Nonequilibrium Green functions allow, at least in principle, the analysis of high frequencies and far-from equilibrium situations. Here we will briefly review recent progress within this formulation. Stafford discussed the current partition in dc but under nonlinear conditions⁴⁸, and recent work by Anantram and Datta⁴⁹ and Wang et al.⁵⁰ have led to an ac generalization. Concerning the tunneling contribution, it is a trivial matter to generalize from the two-probe geometry to a multiprobe system: one merely replaces the indices L, R by α , where α labels the probes, and considers the current $J_\alpha(t)$ (or $J_\alpha(\omega)$, whichever is more convenient). The dynamic conductance $G_{\alpha\beta}$ due to the tunneling current is defined as

$$J_\alpha(\omega) = \sum_\beta G_{\alpha\beta}(\omega)V_\beta(\omega). \quad (29)$$

In the time-dependent case the tunneling currents do not add up to zero, due to charge accumulation/depletion. The total current, however, is conserved:

$$\sum_\alpha J_\alpha(\omega) = i\omega Q(\omega), \quad (30)$$

where

$$Q(\omega) = - \sum_\beta iq \int \frac{dE}{2\pi} \text{Tr}[g_\beta^<(E + \omega, E)]V_\beta \quad (31)$$

is the accumulated charge in the scattering region; $g_{\beta}^{<}(E, E')$ is the double Fourier transform of the *small signal* component of the full Green function $G^{<}$, See Refs.[^{49,50}]. The total current in probe α is $J_{\alpha}^{\text{tot}} = J_{\alpha} + J_{\alpha}^d$, where $\sum_{\alpha} J_{\alpha}^d = J^d = dQ/dt$, and current conservation means $\sum_{\alpha} J_{\alpha}^{\text{tot}} = 0$. Additional information is required to partition J^d , because only the sum of the various displacement currents is known via Eq.(30). In a model where coupling constants between the central region and the contacts are independent of energy, one can readily do this partitioning: $J_{\alpha}^d = (\Gamma_{\alpha}/\sum_{\beta} \Gamma_{\beta})J^d$. In a more elaborate model Wang et al.⁵⁰ have outlined a procedure how this partitioning can be carried out; the analysis is based on requirements of charge conservation, $\sum_{\alpha} G_{\alpha\beta}^{\text{tot}} = 0$, and gauge invariance, $\sum_{\beta} G_{\alpha\beta}^{\text{tot}} = 0$. The end result for the dynamical conductance is

$$G_{\alpha\beta}^{\text{tot}}(\omega) = G_{\alpha\beta} - G_{\beta}^d \frac{\sum_{\gamma} G_{\alpha\gamma}}{G_{\gamma}^d}, \quad (32)$$

where

$$G_{\beta}^d = -q\omega \int \frac{dE}{2\pi} \text{Tr}[g_{\beta}^{<}(E + \omega, E)]. \quad (33)$$

The result (32) formally agrees with the scattering matrix results of Büttiker et al.⁴⁶, but now the various terms are expressed in terms of nonequilibrium Green functions, and hence powerful techniques for evaluating them are available. Clearly the final word is not said in this rapidly developing subfield.

4.6 Phase-measurement of a quantum dot

Measuring the phase of a transmission coefficient in contrast to the amplitude (which determines conductance) has become possible only quite recently^{51,52}. The experimental protocol can be summarized as follows: A magneto-transport measurement is performed on an Aharonov–Bohm ring with a quantum dot fabricated in one of its arms. If the quantum dot supports coherent transport, the transmission amplitudes through the two arms interfere. A magnetic field induces a relative phase change, $2\pi\Phi/\Phi_0$, between the two transmission amplitudes, t_0 and \tilde{t}_{QD} , leading to an oscillatory component to the conductance $g(B) = (e^2/h)\mathcal{T}(B)$, with

$$\mathcal{T}(B) = \mathcal{T}^{(0)} + 2\text{Re}\{t_0^* \tilde{t}_{\text{QD}} e^{2\pi i\Phi/\Phi_0}\} + \dots, \quad (34)$$

where Φ is the flux threading the ring, $\Phi_0 = hc/e$ is the flux quantum, and where the dots represent higher harmonics due to multiple reflections. The amplitudes t_0 and \tilde{t}_{QD} give the *coherent* parts of the two sets of paths joining

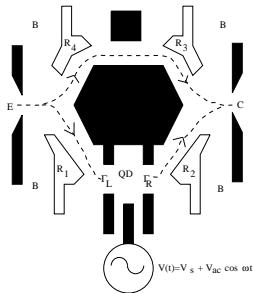


Figure 5: Schematic lay-out of the proposed multi-terminal double-slit interference experiment. The device consists of an Aharonov-Bohm ring with a quantum dot (QD) in one arm, defined with metallic gates (shaded areas) on the 2D electron gas. Electron paths (shown as dashed lines) originating from the emitter (E) interfere at the collector (C). A time-dependent voltage $V(t)$ is applied to the quantum dot via a side gate. The reflector gates $R_{1...4}$, shown as white areas, direct multiply reflected paths to the common base (B), thus preventing them from contributing to the interference signal, in accordance with Eq.(34).

the emitter and the collector; the incoherent components lead to a structureless background signal, which can be neglected in the forthcoming analysis. In the experiments, an oscillatory component in magnetoconductance of this form was clearly observed thus demonstrating coherent transmission through the arm with the dot^{51,52}. In the experiment of Yacoby *et al.*⁵¹, the Aharonov-Bohm phase could take on only two values, 0 and π , as a consequence of microreversibility in a two-terminal geometry. The second generation of experiments⁵², in a four-terminal geometry, allowed the determination of the continuous phase shift of the transmission amplitude through the dot. The success of these experiments suggests applications to other phase-coherent transport processes. One particular example which has been of considerable recent interest is photon-assisted tunneling. While photon-assisted tunneling (PAT) is intrinsically a coherent phenomenon, existing measurements of PAT are insensitive to the phase of the transmitted electrons and do not directly demonstrate coherence in the presence of the time-dependent field. Here we give a brief account of a recent proposal⁵³ for a measurement of photon-assisted tunneling through a quantum dot in the mesoscopic double-slit geometry described above (see Fig. 5). The proposed experiment is a combination of the experiments of Kouwenhoven *et al.*^{54,55} where a microwave modulated side-gate voltage gave rise to photon-assisted tunneling through a quantum dot, and the interference experiments of Refs.⁵¹ and⁵².

We can use the results presented in Section 4.2 to construct an expression for the interference signal. We focus on transport in the neighborhood

of a single Coulomb oscillation peak associated with a single nondegenerate electronic level of the quantum dot. The effect of the ac side-gate voltage is described entirely through the time-dependent energy of this level, which has the familiar form

$$\epsilon(t) = \epsilon_0(V_s) + V_{ac} \cos \omega t, \quad (35)$$

where the static energy of the level ϵ_0 depends on the dc side-gate voltage V_s . All other levels on the dot can be neglected provided the ac amplitude, V_{ac} , and the photon energy, $\hbar\omega$, are small compared to the level spacing on the dot.

The energy-dependence of the coherent part of the transmission amplitude $\tilde{t}_{QD}(\epsilon)$ through the arm containing the quantum dot is determined by the transmission amplitude $t_{QD}(\epsilon)$ through the dot, $\tilde{t}_{QD}(\epsilon) \propto t_{QD}(\epsilon)$. In the absence of an ac potential, a suitable model for the dot transmission amplitude is the Breit–Wigner form,

$$t_{QD}(\epsilon) = \frac{-i\sqrt{\Gamma_L\Gamma_R}}{\epsilon - \epsilon_0(V_s) + i\Gamma/2}, \quad (36)$$

where $\Gamma = \Gamma_L + \Gamma_R$ is the full width at half maximum of the resonance on the dot due to tunneling to the left and right leads. Eq. (36) implies a continuous phase accumulation of π in the transmission amplitude as the Coulomb blockade peak is traversed. (Note that the Breit–Wigner form is exact for a noninteracting system with Γ independent of energy.)

In the dynamic case, the simple Breit–Wigner description must be generalized, and the object to evaluate is the S -Matrix element^{9,41}. Provided interactions in the leads can be neglected, the elastic transmission amplitude $t_{QD}(\epsilon)$ can be written as the energy conserving part of the S -Matrix between the left lead and the right lead

$$\lim_{\epsilon' \rightarrow \epsilon} \langle \epsilon', R | \mathcal{S} | \epsilon, L \rangle = \delta(\epsilon' - \epsilon) t_{QD}(\epsilon), \quad (37)$$

where

$$t_{QD}(\epsilon) = -i\sqrt{\Gamma_L\Gamma_R} \langle A(\epsilon, t) \rangle, \quad (38)$$

with (compare to Sect. 4.3)

$$\langle A(\epsilon, t) \rangle = \sum_{k=-\infty}^{\infty} \frac{J_k^2(V_{ac}/\hbar\omega)}{\epsilon - \epsilon_0(V_s) - k\hbar\omega + i\Gamma/2}. \quad (39)$$

The result for the transmission amplitude at finite temperatures is

$$t_{QD} = \left(-\frac{\Gamma}{4\pi T} \right) \sum_{k=-\infty}^{\infty} J_k^2(V_{ac}/\hbar\omega) \psi' \left[\frac{1}{2} - \frac{i(\mu - \epsilon_0(V_s) - k\hbar\omega + i\frac{\Gamma}{2})}{2\pi k_B T} \right], \quad (40)$$

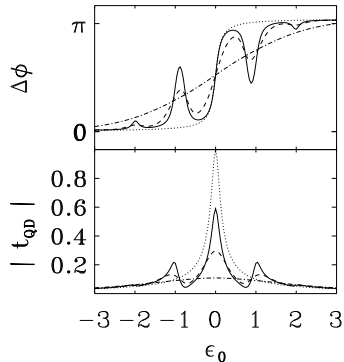


Figure 6: Temperature dependence of the phase shift $\Delta\phi$ (top panel) and the square of the amplitude (bottom) of t_{QD} . The level-width is $\Gamma/2 = 0.1$, in terms of which the other parameters are $V_{ac} = 1.0$, $\omega = 1.0$, and $T = 0$ (solid line), 0.1 (dashed line), 0.5 (dash-dotted line). For comparison, the $T = 0$ time-independent results are shown as dots.

where ψ' is the derivative of the digamma function, and μ is the chemical potential in the leads.

Figure 6 shows the computed magnitude of t_{QD} (bottom) and its phase (top), as a function of the level energy $\epsilon_0(V_s)$. As compared to the time-independent case (shown as a dotted line), several features are noteworthy. The magnitude of t_{QD} shows photonic side-bands, reminiscent of those seen in transmission through a microwave modulated quantum dot⁵⁴. However, there is an important difference from the usual case of photon-assisted tunneling. The amplitude of the Aharonov–Bohm oscillation is sensitive only to the time average of the transmission amplitude t_{QD} . Hence only elastic transmission through the dot contributes, i.e., the net number of photons absorbed from the ac field must be zero. The sideband at say $\epsilon = \epsilon_0(V_s) - \hbar\omega$ corresponds to a process in which an electron first absorbs a photon to become resonant at energy $\epsilon_0(V_s)$, and subsequently reemits the photon to return to its original energy. Perhaps most interesting are the features appearing in the phase: the phase shift shows a non-monotonic behavior, with pronounced resonances located at the energies corresponding to the photonic side-bands. The strengths of these phase resonances are strongly dependent on the ac amplitude V_{ac} , and in Fig. 7 we highlight an interesting consequence of Eq.(40): it is possible to entirely *quench* the main transmission peak (bottom panel), or *change the sign* of the slope of the phase at resonance by adjusting the ratio $V_{ac}/\hbar\omega$ to coincide with a zero of the Bessel function J_0 (top). This phenomenon is mathematically analogous to the recently observed absolute negative conductivity in THz-irradiated superlattices⁵⁶; in our case, however, it is the *phase* rather

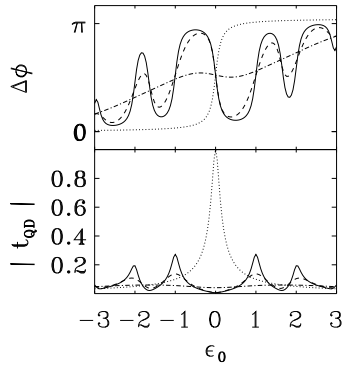


Figure 7: Temperature dependence of the phase shift (top panel) and the amplitude (bottom) of t_{QD} , for $V_{ac} = 2.405$, $\omega = 1.0$, $\Gamma/2 = 0.1$, $T = 0, 0.1, 0.5$.

than the current that displays this behavior. For a reader interested in further developments along these lines, we direct attention to two very recent papers ^{57,58}.

4.7 Time-dependent Kondo physics

The Kondo effect is undoubtedly one of the most studied and best understood problems of many-body physics. Initially, the theory was developed to explain the increase of resistivity of a bulk metal with magnetic impurities at low temperatures ⁵⁹. More recently, the observation of Kondo effect in several experiments on quantum dots ^{60,61} has demonstrated that these systems can serve as an important new tool in the study of strongly correlated systems. Unlike magnetic impurities in metals, the physical parameters of the quantum dot can be varied continuously, which allows, for example, systematic experimental study of the crossover between the Kondo, the mixed-valence, and the non-Kondo regimes. These aforementioned experiments were in good agreement with earlier theoretical predictions ^{62,63,64,65}. It is therefore natural to ask: can Kondo physics be probed in time-dependent experiments? Already before the experiments ^{60,61} a few theoretical papers addressed ac-driven Kondo systems ^{22,67,68,69}, but the last two years have witnessed a flurry of theoretical activity, see, e.g., Refs. ^[70,71,72,18].

A full discussion of these papers would merit a review of its own. Our present goal is however much more modest. This is a rapidly developing area and still ridden with some controversies, which will provide fuel for continued intense research efforts. Important for this volume is that the main technical work-horse has been the nonequilibrium Green function technique. It is there-

fore hoped that the reader will get a feeling of the present excitement from the following brief discussion on some of the recent achievements and open problems related to the ac-Kondo problem.

The static Anderson model is solvable with Bethe Ansatz⁷³ or by quantum Monte Carlo methods⁷⁴, but a reliable and simple method to obtain dynamical properties at low temperatures in the whole range of interactions (U/Γ) is not available. A number of different methods have been used to attack the problem. For example, the non-crossing method (NCA) may be used following an exact transformation of the $U = \infty$ Anderson model into a slave-boson Hamiltonian⁷⁵. The latter is then solved self-consistently to second order in the tunneling matrix elements V_k . The NCA gives reliable results for temperatures down to $T < T_K$, and its time-dependent formulation has been very useful in applications to problems in surface physics^{76,77}. This is the approach of Ref.⁷², which studies the temporal response of a quantum dot which is suddenly shifted into the Kondo regime by a change of a voltage on a nearby gate. Thus, the NCA is applied to a calculation of the nonequilibrium spectral density. It is suggested that subjecting the quantum dot to a sequence of pulses, and analyzing the resulting current as a function of the duration of a pulse, will open a window to the build-up mechanism of the many-body correlations, responsible for the Kondo effect.

NCA, however, does not give exact results as $T \rightarrow 0$, and other methods are called for. Finite U perturbation theory works for the symmetric case, but is known to exhibit anomalies away from this special case. An attempt to circumvent these problems is to construct an effective self-energy, which smoothly interpolates between known limits $U/\Gamma \rightarrow 0$ and $\Gamma/U \rightarrow 0$, and thus may eliminate some of the problems related to perturbative approaches^{78,79}. While a plausible process, interpolation is not rigorous, and the authors of Ref.⁷⁰, suggest a nonequilibrium generalization of the Friedel sum rule to construct a consistency check in the computation of the nonequilibrium Green functions. The resulting time-averaged density-of-states exhibits a rich structure: one may find replicas of the Kondo peak and/or mean-field peaks. Also, the conductivity is found to be strongly affected by the ac-driving, and, interestingly, that it cannot be described by the Tien–Gordon model⁸⁰, i.e., by single-particle ac-assisted tunneling. The observability of the satellites of the Kondo peak is, however, brought into question by Kaminski et al.⁷¹, who point out that the coherence of the many-body correlations responsible for the Kondo anomaly is fragile against a *spin-flip cotunneling* process, which may occur already at relatively low frequencies⁸¹. It is clear that experiments exploring the ac-Kondo system would be extremely welcome!⁸²

4.8 Semiconductor-superconductor hybrid systems

Materials technology has in recent years advanced to a stage where high quality hybrid structures can be fabricated. By hybrid structures we understand combinations of normal metals (N) and superconductors (S) together with mesoscopic structures, such as quantum dots (QD). Thus, in Fig. 2 either of the contacts, or the quantum dot itself could be superconducting. Obviously there are many possible combinations and here we just discuss one of them, namely a N-QD-S structure, recently studied by Sun et al.^{83,84}.

The superconducting contact allows the possibility of an Andreev reflection⁸⁵: an electron approaching the superconductor with subgap energy may be transferred into the condensate with a simultaneous creation of a back-propagating hole. This process reflects itself in a number of ways, for example as bound states in a S-N-S system⁸⁶, or the even-odd parity asymmetry and the Coulomb blockade of the Andreev reflection in S-SQD-S or N-SQD-N systems^{87,88,89,90}. Traditionally rf radiation has been one of the standard probes for studying superconductivity, and a large number of experimental results have been reported on “simple” hybrid systems. Here we discuss the case where a single level (with spin) couples to both radiation and N and S contacts⁸⁴. (It should be noted that a strongly interacting QD in this configuration would bring us again to the Kondo realm⁹¹.) The Hamiltonian is thus $H = H_L(t) + H_{\text{cen}}(t) + H_R + H_{T,L} + H_{T,R}$, where H_L , H_{cen} and $H_{T,L}$ are standard but the presence of the superconductor requires the following modification for the terms referring to the right-hand side of the system:

$$H_R = \sum_{p\sigma} \epsilon_p c_{p\sigma}^\dagger c_{p\sigma} + \sum_p \left[\Delta^* c_{p\downarrow} c_{-p,\uparrow} + \Delta c_{-p,\uparrow}^\dagger c_{p,\downarrow}^\dagger \right] \quad (41)$$

$$H_{T,R} = \sum_{p\sigma} \left[V_k e^{ieV_R t} c_{p\sigma}^\dagger d_\sigma + V_k^* e^{-ieV_R t} d_\sigma^\dagger c_{p\sigma} \right], \quad (42)$$

where the voltage of the superconducting contact V_R appears in the phase of the tunneling coupling⁹². This can be viewed as a mean field Hamiltonian leading to the Bogoliubov–de Gennes equations.

The derivation of the time-dependent current proceeds along the same lines as in Sect. 3. In particular, the central result Eq.(11) is still valid, if one interprets the central region Green functions as Nambu matrices,

$$\mathbf{G}^<(t, t') = i \begin{pmatrix} \langle c_\uparrow^\dagger(t') c_\uparrow(t) \rangle & \langle c_\downarrow(t') c_\uparrow(t) \rangle \\ \langle c_\uparrow^\dagger(t') c_\downarrow^\dagger(t) \rangle & \langle c_\downarrow(t') c^\dagger \downarrow(t) \rangle \end{pmatrix}, \quad (43)$$

and analogous definitions hold for the retarded Green functions and self-energy functionals. The ensuing calculations are quite complicated, even in the case

of a noninteracting quantum dot⁸⁴, and we focus on some of the main physical conclusions. First of all, one must distinguish on what part of the system the time-variation is affecting, and whether the photon energy is bigger or smaller than the energy gap. As an example, let us consider the case when $\hbar\omega < \Delta$, and that the external radiation affects the superconductor (by gauge invariance, this is equivalent to the case when the normal contact *and* the dot are affected, but the superconductor is not). The dominating contribution to the current arises from a photon-assisted Andreev term (PAAT), which has several interesting properties. Among these is a possibility of electron pumping⁹³: the electrons move from a lower potential to higher potential by absorbing photons, leading to a negative current (or, absolute negative conductivity⁵⁶). If, on the other hand, $\hbar > \Delta$, the normal PAT-processes contribute substantially. In general, much interesting structure is seen as a function of the gate voltage, which can be used to tune the energy levels in the quantum dot, and the structure is quite different from the one seen in N-QD-N systems⁹⁴.

5 Concluding remarks

In this review we have attempted to give some insight to recent developments in time-dependent transport in mesoscopic systems, treated by nonequilibrium Green function methods. The review is by no means exhaustive: many important and interesting problems have not been covered, such as noise^{95,96} or surface acoustic wave driven transport⁹⁷ (and there are many other topics as well). The scope of the review has not allowed an in-depth treatment of many of the topics, but the author's hope is that the incomplete treatment has raised the reader's curiosity, and perhaps thereby attracted new researchers into this dynamic field of research.

Acknowledgments

It is a pleasure to thank Hartmut Haug and Ned Wingreen for numerous discussions on nonequilibrium Green functions during various collaborations. I'm also grateful to my group members M. Brandbyge, J. Lægsgaard, and N. A. Mortensen for careful proof-reading, which has substantially reduced the number of inconsistencies in the original draft. The author, of course, bears the full responsibility of the remaining ones.

References

1. C. Caroli, R. Combescot, D. Lederer, P. Nozieres , and D. Saint-James, J .Phys. C **4**, 2598 (1971).
2. C. Caroli, R. Combescot, P. Nozieres, and D. Saint-James, J. Phys. C **4**, 916 (1971).
3. C. Caroli, R. Combescot, P. Nozieres, and D. Saint-James D., J.Phys. C. **5**, 21 (1972).
4. R. Combescot, J. Phys. C **4**, 2611 (1971).
5. H. Haug and A. P. Jauho, *Quantum Kinetics in Transport and Optics of Semiconductors* (Springer Series in Solid-State Sciences, Vol. 123, Springer-Verlag, Berlin Heidelberg, 1996).
6. S. Datta, *Electronic Transport in Mesoscopic Systems*, (Cambridge University Press, Cambridge, 1995).
7. R. Landauer, IBM J. Res. Dev. **1**, 233 (1957).
8. R. Landauer, Philos. Mag. **21**, 863 (1970).
9. A. P. Jauho, N. S. Wingreen, and Y. Meir, Phys. Rev. B **50**, 5528 (1994).
10. G. D. Mahan, *Many-Particle Physics*, Second Edition (Plenum, New York, 1990).
11. A. L. Fetter and J. D. Walecka, *Quantum Theory of Many-Particle Systems* (McGraw-Hill, New York, 1971).
12. C. P. Enz, *A Course on Many-Body Theory Applied to Solid-State Physics* (World Scientific, Singapore, 1992).
13. See, e.g., Ref. 5, Sect. 4.
14. Y. Meir and N. S. Wingreen, Phys. Rev. Lett. **68**, 2512 (1992).
15. B. G. Wang, J. Wang, and H. Guo, J. Appl. Phys. **86**, 5094 (1999).
16. M. B. Nardelli, Phys. Rev. B **60**, 7828 (1999).
17. M. P. Anantram and T. R. Govindan, Phys. Rev. B **58**, 4882 (1998).
18. A. L. Yeyati, F. Flores, and A. Martin-Rodero, Phys. Rev. Lett. **83**, 600 (1999).
19. O. Takagi and T. Saso, J. Phys. Soc. Jpn. **68**, 2894 (1999).
20. O. Sakai, S. Suzuki, W. Izumida, et al., J. Phys. Soc. Jpn. **68**, 1640 (1999).
21. W. B. Thimm, J. Kroha, and J. von Delft, Phys. Rev. Lett. **82**, 2143 (1999).
22. M. H. Hettler, J. Kroha, and S. Hershfield, Phys. Rev. B **58**, 5649 (1998).
23. R. Raimondi and P. Schwab, Superlattices and Microst. **25**, 1141 (1999).
24. C. Heide, Phys. Rev. B **60**, 2571 (1999).
25. R. Berkovits, Phys. Rev. B **60**, 26 (1999).
26. L. Craco and K. C. Kang, Phys. Rev. B **59**, 12244 (1999).

27. H. Akera, Phys. Rev. B **59**, 9802 (1999).
28. A. Georges and Y. Meir, Phys. Rev. Lett. **82**, 3508 (1999).
29. F. Ramirez, E. Cota, and S. E. Ulloa, Phys. Rev. B **59**, 5717 (1999).
30. B. Jonault, M. Boero, G. Faini, et al., Phys. Rev. B **59**, 4966 (1999).
31. C. A. Stafford, R. Kotlyar, and S. Das Sarma, Phys. Rev. B **58**, 7091 (1999).
32. J. Favand and F. Mila, Eur. Phys. J. B **2**, 293 (1998).
33. J. C. Cuevas, A. Levy Yeayati, and A. Martin-Rodero, Phys. Rev. Lett. **80**, 1066 (1998).
34. M. Brandbyge, N. Kobayashi, and M. Tsukada, to appear in Phys. Rev. B **60**, 15 December 1999.
35. G. A. D. Briggs and A. J. Fisher, Surf. Sci. Rep. **33**, 3 (1999).
36. A. L. Vázquez de Parga et al., Phys. Rev. Lett. **80**, 357 (1998).
37. M. Büttiker and R. Landauer, Phys. Rev. Lett. **49**, 1739 (1982).
38. R. Aguado, J. Iñarrea, and G. Platero, Phys. Rev. B **53**, 10030 (1996).
39. V. J. Goldman, D. C. Tsui, and J. E. Cunningham, Phys. Rev. B **36**, 7635 (1987).
40. See, e.g., pp. 285–324 in G. D. Mahan, *Many-Particle Physics*, Second Edition (Plenum, New York, 1990).
41. N. S. Wingreen, K. W. Jacobsen, and J. W. Wilkins, Phys. Rev. B **40**, 11834 (1989).
42. E. V. Anda and F. Flores, J. Phys.: Condens. Matter **3**, 9087 (1991).
43. P. Hylgaard, S. Hershfield, J. H. Davies, and J. W. Wilkins, Ann. Phys. NY **236**, 1 (1994).
44. J. Iñarrea and G. Platero, Phys. Rev. B **51**, 5244 (1995).
45. C. Zhang, M. L. F. Lerch, A. D. Marting, P. E. Simmonds, and L. Eaves, Phys. Rev. Lett. **72**, 3397 (1994).
46. M. Büttiker, Y. Imry, R. Landauer, and S. Pinhas, Phys. Rev. B **31**, 6207 (1985).
47. M. Büttiker, A. Prêtre, and H. Thomas, Phys. Rev. Lett. **70**, 4114 (1993).
48. C. A. Stafford, Phys. Rev. Lett. **77**, 2770 (1996).
49. M. P. Anantram and S. Datta, Phys. Rev. B **51**, 7632 (1995).
50. B. G. Wang, J. Wang, and H. Guo, Phys. Rev. Lett. **82**, 398 (1999).
51. A. Yacoby, M. Heiblum, D. Mahalu, and H. Shtrikman, Phys. Rev. Lett. **74**, 4047 (1995).
52. R. Schuster, E. Buks, M. Heiblum, D. Mahalu, V. Umansky, and H. Shtrikman, Nature **385**, 417 (1997).
53. A. P. Jauho and N. S. Wingreen, Phys. Rev. B **58**, 9619 (1998).
54. L. Kouwenhoven, S. Jauhar, J. Orenstein, P. L. McEuen, Y. Nagamune,

- J. Motohisa, and H. Sakaki Phys. Rev. Lett. **73**, 3443 (1993).
55. T. H. Oosterkamp, L. P. Kouwenhoven, A. E. A. Koolen, N. C. van der Vaart, and C. J. P. M. Harmans, Phys. Rev. Lett. **78**, 1536 (1997).
 56. B. J. Keay, S. Zeuner, S. J. Allen, Jr., K. D. Maranowski, A. C. Gossard, U. Bhattacharya, and M. J. W. Rodwell, Phys. Rev. Lett. **75**, 4102 (1995).
 57. D. S. Citrin, Phys. Rev. B **60**, 5659 (1999).
 58. Q.-f. Sun, J. Wang, T.-h. Lin, to appear in Phys. Rev. B **60**, 15 November 1999.
 59. J. Kondo, Prog. Theor. Phys. **32**, 37 (1964).
 60. D. Goldhaber et al., Nature (London) **391**, 156 (1998); D. Goldhaber et al., Phys. Rev. Lett. **81**, 5225 (1998).
 61. S. M. Cronenwett, T. H. Oosterkamp, and L. P. Kouwenhoven, Science **281**, 540 (1998).
 62. L. I. Glazman and M. E. Raikh, Pis'ma Zh. Eksp. Teor. Fiz. **47**, 378 (1988) [JETP Lett. **47**, 452 (1988)].
 63. T. K. Ng and P. A. Lee, Phys. Rev. Lett. **61**, 1768 (1988).
 64. S. Hershfield, J. H. Davies, and J. W. Wilkins, Phys. Rev. Lett. **67**, 3720 (1991).
 65. Y. Meir, N. S. Wingreen, and P. A. Lee, Phys. Rev. Lett. **70**, 2601 (1993).
 66. M. H. Hettler and H. Schoeller, Phys. Rev. Lett. **74**, 4907 (1995).
 67. A. Schiller and S. Hershfield, Phys. Rev. Lett. **77**, 1821 (1996).
 68. T. K. Ng, Phys. Rev. Lett. **76**, 487 (1996).
 69. Y. Goldin and Y. Avishai, Phys. Rev. Lett. **81**, 5394 (1998).
 70. R. Lopez, R. Aguado, G. Platero, and C. Tejedor, Phys. Rev. Lett. **81**, 4688 (1998).
 71. A. Kaminski, Yu. V. Nazarov, and L. I. Glazman, Phys. Rev. Lett. **83**, 384 (1999).
 72. P. Nordlander, M. Pustilnik, Y. Meir, N. S. Wingreen, and D. C. Langreth, Phys. Rev. Lett. **83**, 808 (1999).
 73. A. M. Tsvelik and P. B. Wiegmann, Adv. Phys. **32**, 453 (1983).
 74. R. M. Fye and J. E. Hirsch, Phys. Rev. B. **38**, 433 (1988).
 75. N. E. Bickers, Rev. Mod. Phys. **59**, 845 (1987).
 76. D. C. Langreth and P. Nordlander, Phys. Rev. B **43**, 2541 (1991).
 77. H. Shao, D. C. Langreth, and P. Nordlander, Phys. Rev. B. **49**, 13929 (1994).
 78. A. Levi Yeyati et al., Phys. Rev. Lett. **71**, 2991 (1993).
 79. H. Kajuter and G. Kotliar, Phys. Rev. Lett. **77**, 131 (1996).
 80. P. K. Tien and J. Gordon, Phys. Rev. **129**, 647 (1963).

81. Similar results have been obtained by a NCA-based numerical calculation, P. Nordlander et al., cond-mat/9801241, and Phys. Rev. B., January 15, 2000.
82. The author is aware of a recent preprint by J. M. Eizerman et al., who study the microwave suppression of the Kondo effect in quantum dots. This experiment did not show ac-Kondo sidebands.
83. Q.-f. Sun, J. Wang, and T.-h. Lin, Phys. Rev. B **59**, 3831 (1999).
84. Q.-f. Sun, J. Wang, and T.-h. Lin, Phys. Rev. B **59**, 13126 (1999).
85. A. F. Andreev, Zh. Eksp. Teor. Fiz. **46**, 1823 (1964) [Sov. Phys. JETP **19**, 1228 (1964)].
86. A. F. Morpurgo, S. Holl, B. J. Van Wees, T. M. Klapwijk, and G. Borghs, Phys. Rev. Lett. **78**, 2636 (1997).
87. M. T. Tuominen, J. M. Hergenrother, T. S. Tighe, and M. Tinkham, Phys. Rev. Lett. **69**, 1997 (1992).
88. T. M. Eiles, J. M. Martinis, and M. H. Devoret, Phys. Rev. Lett. **70**, 1862 (1993).
89. F. W. J. Hekking, L. I. Glazman, K. A. Matveev, and R. I. Shekhter, Phys. Rev. Lett. **70**, 4138 (1993).
90. J. M. Hergenrother, M. T. Tuominen, and M. Tinkham, Phys. Rev. Lett. **72**, 1742 (1994).
91. R. Fazio and R. Raimondi, Phys. Rev. Lett. **80**, 2913 (1998).
92. J. C. Cuevas, A. Martin-Rodero, and A. Levy Yeyati, Phys. Rev. B **54**, 7366 (1996).
93. A similar effect in a double quantum well has been discussed by C. A. Stafford and N. S. Wingreen, Phys. Rev. Lett. **76**, 1916 (1996).
94. L. P. Kouwenhoven et al., Phys. Rev. Lett. **73**, 3443 (1994).
95. L. Y. Chen and C. S. Ting, Phys. Rev. B **46**, 4714 (1992).
96. J. C. Cuevas, A. Martin-Rodero, and A. Levy Yeayati, Phys. Rev. Lett. **82**, 4086 (1999).
97. K. Flensberg, Q. Niu, and M. Pustilnik, to appear in Phys. Rev. B **60**, 15 December 1999.